Modeling two-dimensional anisotropic photonic crystals by Dirichlet-to-Neumann maps

Huan Xie[1,2,3,*] and Ya Yan Lu[3]

[1] *Joint Advanced Research Center of University of Science and Technology of China and City University of Hong Kong, Suzhou, Jiangsu, China*

[2] *Department of Mathematics, University of Science and Technology of China Hefei, Anhui, China*

[3] *Department of Mathematics, City University of Hong Kong, Kowloon, Hong Kong*

[*] *Corresponding author: xiehuan@mail.ustc.edu.cn*

For photonic crystals (PhCs) and related devices, it is useful to calculate the Dirichlet-to-Neumann (DtN) map of a unit cell which maps the wave field to its normal derivative on the boundary. The DtN map can be used to avoid further calculations in the interiors of the unit cells and formulate mathematical problems on the cell boundaries. In this paper, we develop a method to approximate the DtN map for two-dimensional PhCs involving anisotropic media, and calculate band structures for PhCs involving liquid crystals. For band structures of triangular lattice PhCs, we also develop new eigenvalue problem formulations involving smaller matrices.

OCIS codes: 000.4430, 050.5298.

1. Introduction

In the last two decades, photonic crystals (PhCs) [1] have attracted much attention because of their amazing ability to manipulate and control light. Due to a periodicity on the scale of the optical wavelength, PhCs exhibit unusual dispersion properties and frequency intervals (i.e., bandgaps) in which light cannot propagate. Numerous PhC devices and components utilizing the bandgap and special dispersion effects have been designed and fabricated. PhCs composed of anisotropic materials have also been studied [2–10]. In particular, liquid crystals have been used in PhCs to obtain tunability of the band structures [4–9]. For practical applications, it is highly desirable to dynamically change the bandgaps, and liquid crystals can achieve this through their electro-optic and thermal effects.

To understand the basic physical properties of a PhC and to design PhC devices for various applications, efficient numerical methods are needed. Mathematically, we encounter eigenvalue problems for band structures, PhC waveguides and PhC microcavities, and also boundary value problems for

PhCs of finite size and PhC devices such as waveguide bends, branches, couplers, interferometers, etc. For band structures, the standard formulation gives rise to an eigenvalue problem on the unit cell, where the eigenvalue is the frequency [1]. PhC waveguides and microcavities are often analyzed using the supercell approach. A matrix eigenvalue problem is obtained when the problem is discretized by a numerical method [11–14]. However, the resulting matrices can be quite large, especially for PhC waveguides and microcavities when the supercell approach is used. The eigenvalue problem becomes nonlinear and more difficult to solve when the PhC is composed of dispersive materials. To analyze general PhC devices, the finite difference time domain (FDTD) method [15] is widely used. However, FDTD often requires prohibitive computer resources including both CPU time and computer memory. The accuracy can often be limited due to poor resolution of material interfaces, improper truncation of periodic structures that extend to infinity, etc.

Recently, various PhC structures have been analyzed using numerical methods that rely on the Dirichlet-to-Neumann (DtN) maps of the unit cells [16–22]. For a unit cell Ω with boundary $\partial\Omega$, the DtN map Λ is an operator (which can be approximated by a small matrix) that maps the wave field on $\partial\Omega$ to the normal derivative of the field on $\partial\Omega$. For band structures [16, 17] and PhC waveguides [18], the DtN map approach is used together with alternative formulations for which the eigenvalue is related to the Bloch wave vector. These eigenvalue problems are linear even when the medium is dispersive, and they are formulated on the edges of the unit cells (or supercells for PhC waveguides), so that the matrices appeared in discrete approximations are much smaller. The advantage of the DtN approach is even more evident for boundary value problems [20–22]. Although a general PhC device can be quite complicated, it still has a background lattice structure and has only a small number of distinct (regular or defect) unit cells. Based on the DtN maps of the unit cells, it is possible to avoid the interiors of the unit cells and solve the wave field on the edges of the unit cells only. Furthermore, the equation on each interior edge is only related to the edges of the two neighboring unit cells, therefore the system of equations on the edges is in fact a sparse linear system [22].

So far, the DtN map approach has only been developed for two-dimensional (2D) PhCs composed of isotropic materials. In this paper, we extend the DtN map technique to 2D anisotropic PhCs. In Section 3, we construct DtN maps for 2D unit cells with circular cylinders involving anisotropic media. In Sections 4 and 5, we apply the DtN maps to calculate band structures of 2D anisotropic PhCs. The anisotropy reduces symmetry and enlarges the irreducible Brillouin zone. For PhCs composed of cylinders in a triangular lattice, while the original formulations developed in [17] are still applicable, we introduce new formulations that give rise to smaller matrices. In Section 5, we demonstrate our method by numerical examples involving liquid crystals.

2. Basic equations

We consider ideal 2D photonic crystals composed of infinitely long and circular cylinders arranged as a square or triangular lattice embedded in a homogeneous background medium, where the axes of the cylinders are parallel to the z axis. We also assume that the electromagnetic waves are propagating in the xy plane, so that the z-derivatives of the electromagnetic fields vanish. For

isotropic media, these assumptions lead to the separation of E and H polarizations, where the time harmonic Maxwell's equations can be reduced to Helmholtz equations for E_z and H_z, respectively. For a general anisotropic medium, such a reduction to two separate polarizations is no longer possible, thus a full-vectorial study is needed even for this ideal 2D problem [23, 24].

On the other hand, if the z-axis is one of the principle axes of the anisotropic medium, it is again possible to separate the E and H polarizations [14, 25]. In the Cartesian coordinate system $\{x, y, z\}$, the relative permittivity matrix ε of an anisotropic medium is a 3×3 symmetric matrix. If the z-axis is a principle axis, we have

$$\varepsilon = \begin{bmatrix} \varepsilon_{11} & \varepsilon_{12} & 0 \\ \varepsilon_{21} & \varepsilon_{22} & 0 \\ 0 & 0 & \varepsilon_3 \end{bmatrix}, \tag{1}$$

where $\varepsilon_{12} = \varepsilon_{21}$. Within a unit cell of an anisotropic PhC, there are two homogeneous media (inside and outside the cylinder, respectively), therefore we need a position dependent relative permittivity matrix $\varepsilon = \varepsilon(\mathbf{x})$ for $\mathbf{x} = (x, y)$, and Eq. (1) is assumed to be valid for both media. From the time harmonic Maxwell's equations for linear, homogeneous (no sources), non-magnetic and anisotropic media, it is straightforward to derive the following scalar equations for the z-components of the electromagnetic fields:

$$\nabla^2 E_z + k_0^2 \varepsilon_3(\mathbf{x}) E_z = 0, \tag{2}$$

$$\nabla \cdot \left(\varepsilon_*^{-1}(\mathbf{x}) \nabla H_z \right) + k_0^2 H_z = 0, \tag{3}$$

where $k_0 = \omega/c$ is the free space wavenumber, ω is the angular frequency, c is the speed of light in vacuum, $\nabla = [\partial_x, \partial_y]$ is the 2D gradient operator, $\nabla^2 = \partial_x^2 + \partial_y^2$ is the 2D Laplacian, $\nabla\cdot$ is the 2D divergence operator and

$$\varepsilon_* = \begin{bmatrix} \varepsilon_{22} & -\varepsilon_{21} \\ -\varepsilon_{12} & \varepsilon_{11} \end{bmatrix}. \tag{4}$$

A more explicit version of Eq. (3) can be obtained if we write down ε_*^{-1} analytically and expand the first term in (3) as a sum of four terms [14]. Since Eq. (2) for the E polarization is identical to the governing equation of isotropic media, we concentrate on the H polarization in the following sections.

3. DtN map of a unit cell

In earlier work for 2D PhCs of isotropic media, the DtN maps of the unit cells were used to derive efficient numerical methods for calculating band structures [16, 17], waveguide modes [18], microcavity modes [19], transmission and reflection spectra of finite PhCs [20, 21] and analyzing general PhC devices [22]. Typical unit cells for square and triangular lattices are shown in Fig. 1. For 2D PhCs of anisotropic media and the H polarization, the DtN map of a unit cell Ω is the operator Λ satisfying

$$\Lambda H_z = \frac{\partial H_z}{\partial \nu} \quad \text{on} \quad \partial\Omega, \tag{5}$$

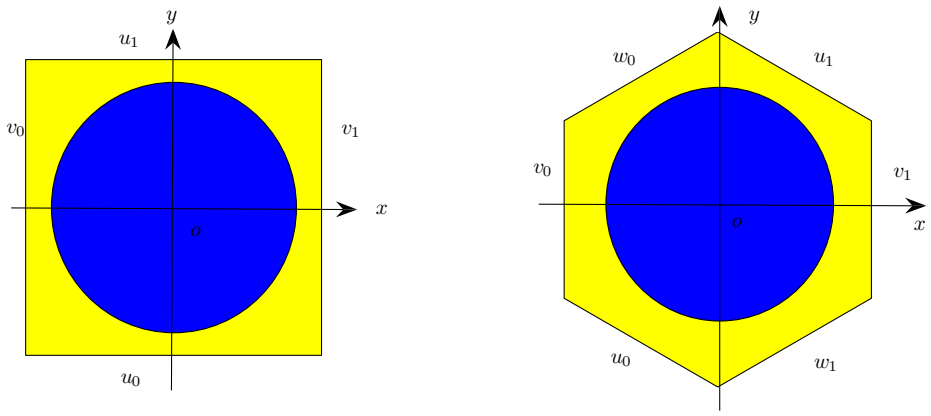

Fig. 1. Square and hexagon unit cells for square and triangular lattices, respectively.

where $\partial\Omega$ is the boundary of Ω, $\nu = \nu(\mathbf{x})$ is a unit normal vector of $\partial\Omega$ at $\mathbf{x} \in \partial\Omega$, and H_z is an arbitrary solution of Eq. (3). To extend the DtN map methods to PhCs with anisotropic media, we need an accurate and efficient method to compute matrix approximations of Λ.

Using the procedure first developed in [20], we construct approximate DtN maps based on special solutions of the governing equation. If we choose K sampling points on $\partial\Omega$ and approximate the general solution of Eq. (3) by a sum of K special solutions, then the DtN map Λ can be approximated by a $K \times K$ matrix. More precisely, we approximate the general solution of Eq. (3) by

$$H_z(\mathbf{x}) \approx \sum_{m=1}^{K} c_m \Phi_m(\mathbf{x}), \tag{6}$$

where Φ_m, for $1 \le m \le K$, are special solutions of (3). Choosing K sampling points on $\partial\Omega$ as $\mathbf{x}_l$ for $1 \le l \le K$, we calculate two $K \times K$ matrices Λ_1 and Λ_2 whose (l, m) entries are $\Phi_m(\mathbf{x}_l)$ and $\partial_\nu \Phi_m(\mathbf{x}_l)$, respectively, where $\nu = \nu(\mathbf{x}_l)$ is the unit normal vector of $\partial\Omega$ at $\mathbf{x}_l$, then the DtN map is approximated by the matrix $\Lambda = \Lambda_2 \Lambda_1^{-1}$. For 2D PhCs of isotropic media, if the unit cell contains a circular cylinder, the special solutions are available analytically as the cylindrical waves [20]. If the cylinder has an arbitrary cross section, the special solutions can be obtained by solving a boundary integral equation [26].

For unit cells with anisotropic media, we need to find special solutions of Eq. (3). Let us consider a unit cell Ω that contains a circular cylinder of radius a. Although both media inside and outside the cylinder can be anisotropic in general, we first consider the case where only the medium inside the cylinder is anisotropic. Inside the cylinder, we can diagonalize the leading 2×2 block of the relative permittivity matrix, rotate and re-scale the coordinates so that Eq. (3) is reduced to the standard Helmholtz equation. More precisely, we assume

$$\begin{bmatrix} \varepsilon_{11} & \varepsilon_{12} \\ \varepsilon_{21} & \varepsilon_{22} \end{bmatrix} = Q \begin{bmatrix} \varepsilon_1 & \\ & \varepsilon_2 \end{bmatrix} Q^T, \tag{7}$$

where ε_1 and ε_2 are the two eigenvalues, Q is a 2×2 orthogonal matrix whose columns are the corresponding eigenvectors and Q^T is the transpose of Q. Assuming that the first eigenvector forms an angle of ϕ with the x axis, then Q can be written as

$$Q = \begin{bmatrix} \cos\phi & -\sin\phi \\ \sin\phi & \cos\phi \end{bmatrix}. \tag{8}$$

Assuming that the origin of the xy coordinate system is at the center of the anisotropic cylinder and (r, θ) is the corresponding polar coordinates, we can rotate the coordinates by angle ϕ and obtain the new Cartesian coordinates (x', y') by

$$\begin{bmatrix} x' \\ y' \end{bmatrix} = \begin{bmatrix} r\cos(\theta - \phi) \\ r\sin(\theta - \phi) \end{bmatrix} = Q^T \begin{bmatrix} x \\ y \end{bmatrix}.$$

Meanwhile, Eq. (3) becomes

$$\nabla' \cdot \left(Q^T \varepsilon_*^{-1} Q \nabla' H_z \right) + k_0^2 H_z = 0, \tag{9}$$

where $\nabla' = [\partial'_x, \partial'_y]$. From (7), we can deduce that

$$Q^T \varepsilon_*^{-1} Q = \begin{bmatrix} \varepsilon_2^{-1} & \\ & \varepsilon_1^{-1} \end{bmatrix}.$$

Therefore, Eq. (9) is simplified to

$$\frac{\partial}{\partial x'} \left(\frac{1}{\varepsilon_2} \frac{\partial H_z}{\partial x'} \right) + \frac{\partial}{\partial y'} \left(\frac{1}{\varepsilon_1} \frac{\partial H_z}{\partial y'} \right) + k_0^2 H_z = 0. \tag{10}$$

We can define the stretched coordinates by $\hat{x} = \sqrt{\varepsilon_2}\, x'$ and $\hat{y} = \sqrt{\varepsilon_1}\, y'$, then Eq. (10) is reduced to the standard Helmholtz equation

$$\frac{\partial^2 H_z}{\partial \hat{x}^2} + \frac{\partial^2 H_z}{\partial \hat{y}^2} + k_0^2 H_z = 0. \tag{11}$$

Furthermore, we can define the stretched polar coordinators $(\hat{r}, \hat{\theta})$ such that $\hat{x} = \hat{r}\cos\hat{\theta}$ and $\hat{y} = \hat{r}\sin\hat{\theta}$, then $\hat{r} = r\hat{n}$, where $\hat{n}$ and $\hat{\theta}$ are functions of $\theta' = \theta - \phi$ satisfying

$$\hat{n}^2 = \varepsilon_1 \sin^2\theta' + \varepsilon_2 \cos^2\theta', \quad \tan\hat{\theta} = \sqrt{\frac{\varepsilon_1}{\varepsilon_2}} \tan\theta'. \tag{12}$$

Therefore, from the standard cylindrical wave solutions of Eq. (11), we obtain a special solution in the anisotropic cylinder:

$$\Phi_m(\mathbf{x}) = J_m(k_0 \hat{n} r) e^{im\hat{\theta}}, \quad r < a, \tag{13}$$

where m is an integer and J_m is a Bessel of the first kind.

Outside the cylinder, we assume that the medium is isotropic with a constant refractive index n_0. Therefore, the special solution can be given in the following Fourier-Bessel expansion:

$$\Phi_m(\mathbf{x}) = \sum_{j=-\infty}^{\infty} \left[a_j^{(m)} J_j(k_0 n_0 r) + b_j^{(m)} Y_j(k_0 n_0 r) \right] e^{ij\theta}, \quad r > a, \tag{14}$$

where Y_j is a Bessel function of the second kind, $\{a_j^{(m)}, b_j^{(m)}\}$ are coefficients to be determined. For the H polarization satisfying Eq. (3), H_z and the tangential component of the electric field must be continuous at any material interface. The latter condition gives rise to the continuity of $\nu \cdot \varepsilon_*^{-1} \nabla H_z$, where ν is a normal vector of the interface. On the boundary of the circular cylinder and using the rotated coordinates introduced earlier, we have $\nu = (\cos\theta, \sin\theta)$ and

$$\nu \cdot \varepsilon_*^{-1} \nabla H_z = \frac{\cos\theta'}{\varepsilon_2} \frac{\partial H_z}{\partial x'} + \frac{\sin\theta'}{\varepsilon_1} \frac{\partial H_z}{\partial y'}.$$

Therefore, the continuity of the tangential component of the electric field gives rise to

$$\frac{1}{n_0^2} \frac{\partial H_z}{\partial r}\bigg|_{r=a^+} = \left(\frac{\cos\theta'}{\varepsilon_2} \frac{\partial H_z}{\partial x'} + \frac{\sin\theta'}{\varepsilon_1} \frac{\partial H_z}{\partial y'} \right)\bigg|_{r=a^-}. \tag{15}$$

For the special solution Φ_m given in (13), the right hand side above becomes

$$\begin{aligned} W_m(\mathbf{x}) &= \frac{\cos\theta'}{\varepsilon_2} \frac{\partial \Phi_m}{\partial x'} + \frac{\sin\theta'}{\varepsilon_1} \frac{\partial \Phi_m}{\partial y} \\ &= e^{im\hat{\theta}} \left[\frac{k_0}{\hat{n}} J_m'(k_0 \hat{n} r) + \frac{im(\varepsilon_2 - \varepsilon_1)\sin(2\theta')}{2r\hat{n}^2\sqrt{\varepsilon_1\varepsilon_2}} J_m(k_0\hat{n}r) \right]. \end{aligned}$$

If we write down the Fourier series of Φ_m and W_m at $r = a^-$:

$$J_m(k_0\hat{n}a)\, e^{im\hat{\theta}} = \sum_{j=-\infty}^{\infty} \hat{V}_j^{(m)}\, e^{ij\theta}, \quad W_m|_{r=a} = \sum_{j=-\infty}^{\infty} \hat{W}_j^{(m)}\, e^{ij\theta},$$

then the coefficients $a_j^{(m)}$ and $b_j^{(m)}$ can be solved from the following 2×2 system:

$$\begin{bmatrix} J_j(k_0 n_0 a) & Y_j(k_0 n_0 a) \\ J_j'(k_0 n_0 a) & Y_j'(k_0 n_0 a) \end{bmatrix} \begin{bmatrix} a_j^{(m)} \\ b_j^{(m)} \end{bmatrix} = \begin{bmatrix} \hat{V}_j^{(m)} \\ \frac{n_0}{k_0} \hat{W}_j^{(m)} \end{bmatrix}. \tag{16}$$

In practice, we can discretize θ by J points, use discrete Fourier transform to find approximate values of $\hat{V}_j^{(m)}$ and $\hat{W}_j^{(m)}$, then solve the coefficients $a_j^{(m)}$ and $b_j^{(m)}$. In that case, the integer j is truncated to $-J/2 \le j < J/2$ if J is even, or $-(J-1)/2 \le j \le (J-1)/2$ if J is odd.

The above construction for the special solutions can be generalized to the case where the medium outside the cylinder is also anisotropic, as far as the relative permittivity matrix ε has the form (1) for both media inside and outside the cylinder. In that case, we rotate and re-scale the axes for the medium outside the cylinder and define two new functions $\hat{n}_{ext}$ and $\hat{\theta}_{ext}$ similar to those given in (12), then the special solution outside the cylinder is obtained by replacing n_0 and θ in (14) by $\hat{n}_{ext}$ and $\hat{\theta}_{ext}$, respectively. To find the coefficients $\{a_j^{(m)}, b_j^{(m)}\}$, we expand the interior solutions Φ_m and W_m in Fourier series of $\hat{\theta}_{ext}$ instead of θ.

After the special solutions are obtained, we can find the DtN map of the unit cell by the method described earlier. However, a modification to (6) is necessary, namely, the integer m should be truncated to $-K/2 \le m < K/2$, when K is an even integer. For square or hexagon unit cells, we typically use N points on each edge, therefore, the total number of points on the boundary of a square or hexagon unit cell is $4N$ or $6N$, and it is always even.

4. Eigenvalue problems

To compute band structures for PhCs with anisotropic materials, existing techniques such as the finite element method [14] and the plane wave expansion method [11], require a full discretization of the unit cell that leads to eigenvalue problems of relatively large matrices. For PhCs with isotropic materials, an alternative method was developed using the DtN maps of the unit cells [16, 17, 26]. The DtN map method formulates eigenvalue problems on the boundary of a unit cell, therefore the resulting matrices are much smaller. Furthermore, it gives rise to linear eigenvalue problems even when the medium is dispersive. The formulations developed in [16, 17, 26] are applicable to PhCs involving anisotropic media, if we use the DtN map constructed in Section 3. In this section, we present new formulations that produce even smaller matrices for PhCs composed of cylinders on a triangular lattice.

For band structure analysis, we look for Bloch waves given by

$$H_z(\mathbf{x}) = \Psi(\mathbf{x}) \exp(i\alpha x + i\beta y), \tag{17}$$

where Ψ is a periodic function of $\mathbf{x}$ following the lattice structure of the PhC, and (α, β) is the Bloch wave vector. These solutions only exist when ω, α and β satisfy the dispersion relations. The wave vector (α, β) can be restricted to the irreducible Brillouin zone. For anisotropic media, the irreducible Brillouin zones for both square and triangular lattices are shown in Fig. 2. They

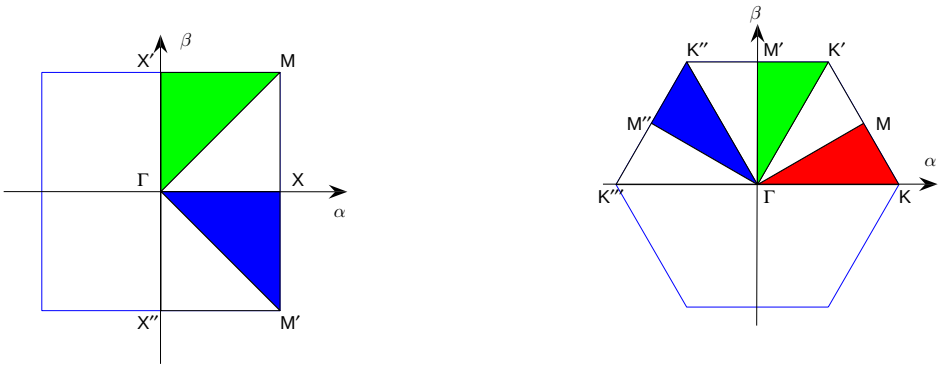

Fig. 2. Left: Irreducible Brillouin zone of square lattice; Right: Irreducible Brillouin zone for a triangular lattice.

are larger than the corresponding zones for isotropic media due to a breaking of symmetry [25]. In the standard approach [1], we assume that a real Bloch wave vector (α, β) is given, then solve ω (or ω^2) as the eigenvalues from the governing equation (3) defined on the unit cell, subject to quasi-periodic conditions derived from the special form of the solution given in (17). In the DtN map method, we assume ω is a given parameter and solve eigenvalue problems where the eigenvalue is related to (α, β).

For a square lattice which is periodic in both x and y directions with a period L (the lattice constant), we consider the square unit cell Ω shown in Fig. 1. Let H_z be an arbitrary solution of the Helmholtz equation (3) in Ω, we denote H_z on the four edges (lower, left, upper and right edges) by u_0, v_0, u_1 and v_1, respectively, then the DtN map Λ satisfies

$$\Lambda \begin{bmatrix} u_0 \\ v_0 \\ u_1 \\ v_1 \end{bmatrix} = \begin{bmatrix} \Lambda_{11} & \Lambda_{12} & \Lambda_{13} & \Lambda_{14} \\ \Lambda_{21} & \Lambda_{22} & \Lambda_{23} & \Lambda_{24} \\ \Lambda_{31} & \Lambda_{32} & \Lambda_{33} & \Lambda_{34} \\ \Lambda_{41} & \Lambda_{42} & \Lambda_{43} & \Lambda_{44} \end{bmatrix} \begin{bmatrix} u_0 \\ v_0 \\ u_1 \\ v_1 \end{bmatrix} = \begin{bmatrix} \partial_y u_0 \\ \partial_x v_0 \\ \partial_y u_1 \\ \partial_x v_1 \end{bmatrix}, \tag{18}$$

where $\partial_y u_0$ denotes $\partial_y H_z$ evaluated on the lower edge of Ω, etc. The DtN map Λ is given in 4×4 blocks, where each block is an $N \times N$ matrix. If H_z is the Bloch wave given in (17), we have the following quasi-periodic conditions:

$$v_1 = \rho_1 v_0, \quad \partial_x v_1 = \rho_1 \partial_x v_0, \tag{19}$$

$$u_1 = \rho_2 u_0, \quad \partial_y u_1 = \rho_2 \partial_y u_0, \tag{20}$$

where $\rho_1 = \exp(i\alpha L)$ and $\rho_2 = \exp(i\beta L)$.

In previous work [16, 26], eigenvalue problems are formulated for edges and diagonals of the irreducible Brillouin zone. In general, we can formulate an eigenvalue problem for any horizontal or vertical line in the $\alpha\beta$ plane, and for any line that is parallel to one of the diagonals of the first Brillouin zone. Consider a vertical line where α is a constant, we can formulate an eigenvalue problem where ρ_2 is the eigenvalue. Since α is given, we can use the quasi-periodic condition (19) to eliminate v_0, v_1, $\partial_x v_0$ and $\partial_x v_1$ in (18), and find the reduced DtN map M satisfying

$$M \begin{bmatrix} u_0 \\ u_1 \end{bmatrix} = \begin{bmatrix} M_{11} & M_{12} \\ M_{21} & M_{22} \end{bmatrix} \begin{bmatrix} u_0 \\ u_1 \end{bmatrix} = \begin{bmatrix} \partial_y u_0 \\ \partial_y u_1 \end{bmatrix}, \tag{21}$$

where M is also given in 2×2 blocks. Next, we use the quasi-periodic condition (20) to eliminate u_1 and $\partial_y u_1$ in (21). This leads to the following eigenvalue problem:

$$\begin{bmatrix} M_{11} & -I \\ M_{21} & 0 \end{bmatrix} \begin{bmatrix} u_0 \\ \partial_y u_0 \end{bmatrix} = \rho_2 \begin{bmatrix} -M_{12} & 0 \\ -M_{22} & I \end{bmatrix} \begin{bmatrix} u_0 \\ \partial_y u_0 \end{bmatrix}, \tag{22}$$

where I is the $N \times N$ identity matrix. The case of a horizontal line in the $\alpha\beta$ plane is similar, we obtain an eigenvalue problem for eigenvalue ρ_1 and eigenvector $[v_0, \partial_x v_0]^T$. For the line $\beta = \beta_0 + \alpha$, where β_0 is a given constant, we have $\rho_2 = e^{i\beta_0 L}\rho_1$. Therefore, we can use the quasi-periodic conditions to eliminate u_1, v_1, $\partial_y u_1$ and $\partial_x v_1$ in (18), and obtain an eigenvalue problem for eigenvalue ρ_1 and eigenvector $[u_0, v_0, \partial_y u_0, \partial_x v_0]^T$. Finally, for the line $\beta = \beta_0 - \alpha$, we have $\rho_2^{-1} = e^{-i\beta_0 L}\rho_1$. Therefore, we use the quasi-periodic conditions to eliminate v_1, $\partial_x v_1$, u_0 and $\partial_y u_0$ in (18), and obtain an eigenvalue problem for eigenvalue ρ_1 and eigenvector $[v_0, u_1, \partial_x v_0, \partial_y u_1]^T$.

For triangular lattices, we prefer to use the hexagon unit cell shown in Fig. 1 due to its better symmetry. In [17], eigenvalue problems are formulated for various edges of the irreducible Brillouin zone based on the DtN map of the hexagon unit cell. These linear eigenvalue problems involve

$(12N)\times(12N)$ matrices, where N is the number of sampling points on each edge. Our formulations below involve $(4N)\times(4N)$ or $(8N)\times(8N)$ matrices. We introduce three unit vectors

$$\mathbf{a}_1 = (1/2, \sqrt{3}/2), \quad \mathbf{a}_2 = (1, 0), \quad \mathbf{a}_3 = (1/2, -\sqrt{3}/2),$$

and assume that the PhC (or the relative permittivity ε) is periodic in all these three directions with period L (the lattice constant). Although only two directions are needed to define the periodicity (noticing that $\mathbf{a}_3 = \mathbf{a}_2 - \mathbf{a}_1$), we use all three vectors for better symmetry. For the hexagon unit cell shown in Fig. 1, we denote H_z on the six edges by u_0, v_0, w_0, u_1, v_1 and w_1, respectively. Furthermore, the unit normal vector ν of the two edges corresponding to u_0 and u_1 is chosen to be exactly $\mathbf{a}_1$. Similarly, we choose $\mathbf{a_2}$ to be the unit normal vector for edges associated with v_0 and v_1, and $\mathbf{a}_3$ to be the unit normal vector for edges associated with w_0 and w_1. Using these notations, the DtN map of the hexagon unit cell satisfies

$$\Lambda \begin{bmatrix} u_0 \\ v_0 \\ w_0 \\ u_1 \\ v_1 \\ w_1 \end{bmatrix} = \begin{bmatrix} \partial_\nu u_0 \\ \partial_\nu v_0 \\ \partial_\nu w_0 \\ \partial_\nu u_1 \\ \partial_\nu v_1 \\ \partial_\nu w_1 \end{bmatrix}, \tag{23}$$

where Λ is a $(6N)\times(6N)$ matrix, u_0, v_0, ..., are column vectors of length N.

We also introduce three dual unit vectors

$$\mathbf{b}_1 = (-\sqrt{3}/2, 1/2), \quad \mathbf{b}_2 = (0, 1), \quad \mathbf{b}_3 = (\sqrt{3}/2, 1/2),$$

then the dispersion relations, i.e., frequency ω as functions of the Bloch wave vector (α, β), are periodic in $\mathbf{b}_1$, $\mathbf{b}_2$ and $\mathbf{b}_3$ with the period $4\pi/(\sqrt{3}L)$. Notice that $\mathbf{a}_j$ is orthogonal to $\mathbf{b}_j$, for $j = 1$, 2, 3. Therefore, we can expand the Bloch wave vector as

$$(\alpha, \beta) = \gamma_j \mathbf{a}_j + \delta_j \mathbf{b}_j, \tag{24}$$

for $1 \le j \le 3$. Next, we formulate eigenvalue problems for straight lines in the $\alpha\beta$ plane, where either γ_j or δ_j is a constant.

For a fixed j and a constant γ_j, Eq. (24) gives a line in the $\alpha\beta$ plane that is parallel to the unit vector $\mathbf{b}_j$. In Fig. 2, the segments $\Gamma M''$, $\Gamma M'$ and ΓM corresponds to $\gamma_j = 0$ for $j = 1$, 2 and 3, respectively. Since γ_j is a constant, the quasi-periodic conditions in the $\mathbf{a}_j$ direction simplify to the multiplication by the constant $\mu_j = \exp(i\gamma_j L)$. For the case $j = 1$, the quasi-periodic conditions in the $\mathbf{a}_1$ direction are

$$u_1 = \mu_1 u_0, \quad \partial_\nu u_1 = \mu_1 \partial_\nu u_0. \tag{25}$$

If we insert the above into (23), we can eliminate u_0 and u_1, and find the reduced DtN map M satisfying

$$M \begin{bmatrix} v_0 \\ w_0 \\ v_1 \\ w_1 \end{bmatrix} = \begin{bmatrix} \partial_\nu v_0 \\ \partial_\nu w_0 \\ \partial_\nu v_1 \\ \partial_\nu w_1 \end{bmatrix}. \tag{26}$$

An explicit formula for M is given in the Appendix. If we partition M in 4×4 blocks as $M=(M_{kl})$ for $1\le k,l\le 4$, then each block is an $N\times N$ matrix. The quasi-periodic conditions in directions $\mathbf{a}_2$ and $\mathbf{a}_3$ depend on the unknown δ_1. We have

$$\tau_1\, v_0 = \eta_1\, v_1, \qquad \tau_1\, \partial_\nu v_0 = \eta_1\, \partial_\nu v_1, \tag{27}$$

$$w_0 = \tau_1\, \eta_1\, w_1, \quad \partial_\nu w_0 = \tau_1\, \eta_1\, \partial_\nu w_1, \tag{28}$$

where $\tau_1=\sqrt{\mu_1}=\exp(i\gamma_1 L/2)$ and $\eta_1=\exp(i\sqrt{3}\delta_1 L/2)$. These conditions allow us to eliminate v_0, w_0, $\partial_\nu v_0$ and $\partial_\nu w_0$ in (26), and obtain the following eigenvalue problem for η_1:

$$\begin{bmatrix} M_{13} & M_{14} & 0 & 0\\ M_{23} & M_{24} & 0 & 0\\ M_{33} & M_{34} & -I & 0\\ M_{43} & M_{44} & 0 & -I \end{bmatrix} \begin{bmatrix} v_1\\ w_1\\ \partial_\nu v_1\\ \partial_\nu w_1 \end{bmatrix} = \eta_1 \begin{bmatrix} -\frac{1}{\tau_1}M_{11} & -\tau_1 M_{12} & \frac{1}{\tau_1}I & 0\\ -\frac{1}{\tau_1}M_{21} & -\tau_1 M_{22} & 0 & \tau_1 I\\ -\frac{1}{\tau_1}M_{31} & -\tau_1 M_{32} & 0 & 0\\ -\frac{1}{\tau_1}M_{41} & -\tau_1 M_{42} & 0 & 0 \end{bmatrix} \begin{bmatrix} v_1\\ w_1\\ \partial_\nu v_1\\ \partial_\nu w_1 \end{bmatrix}, \tag{29}$$

where I is the $N\times N$ identity matrix. The cases for $j=2$ and $j=3$ are similar. For example, if $j=2$, we have $\gamma_2=\alpha$ and $\delta_2=\beta$, and the following quasi-periodic conditions:

$$u_1 = \tau_2\eta_2\, u_0, \qquad v_1 = \mu_2\, v_0, \qquad \eta_2\, w_1 = \tau_2\, w_0, \tag{30}$$

$$\partial_\nu u_1 = \tau_2\eta_2\, \partial_\nu u_0, \quad \partial_\nu v_1 = \mu_2\, \partial_\nu v_0, \quad \eta_2\, \partial_\nu w_1 = \tau_2\, \partial_\nu w_0, \tag{31}$$

where $\tau_2=\exp(i\gamma_2 L/2)$, $\mu_2=\tau_2^2=\exp(i\gamma_2 L)$ and $\eta_2=\exp(i\sqrt{3}\delta_2 L/2)$. If δ_2 is a constant, we can formulate an eigenvalue problem for eigenvalue η_2.

We can also formulate an eigenvalue problem assuming that the Bloch wave vector is given in (24) with a constant δ_j. In that case, Eq. (24) gives a line in the $\alpha\beta$ plane parallel to the unit vector $\mathbf{a}_j$. In the Brillouin zone of the triangular lattice shown in Fig. 2, the line segments ΓK, $\Gamma K'$, $\Gamma K''$, $\Gamma K'''$ and edges KK', $K'K''$ and $K''K'''$ all corresponds to the case considered here for different j and δ_j. Consider the case for $j=1$ again. The quasi-periodic conditions (25), (27) and (28) are still valid. However, this time η_1 is a given constant and τ_1 is the eigenvalue to be determined. Since $\mu_1=\tau_1^2$ shows up in (25), we introduce the extra functions g and $\partial_\nu g$ to linearize the problem:

$$u_1 = \tau_1 g, \quad g = \tau_1 u_0, \quad \partial_\nu u_1 = \tau_1 \partial_\nu g, \quad \partial_\nu g = \tau_1 \partial_\nu u_0. \tag{32}$$

Now, we can insert (27), (28) and (32) into Eq. (23) to eliminate u_1, v_1, w_0, $\partial_\nu u_1$, $\partial_\nu v_1$ and $\partial_\nu w_0$. This gives rise to the following linear eigenvalue problem:

$$A\mathbf{u} = \tau_1 B\mathbf{u}, \tag{33}$$

where $\mathbf{u}=[u_0, v_0, w_1, \partial_\nu u_0, \partial_\nu v_0, \partial_\nu w_1, g, \partial_\nu g]^T$ is a column vector of length $8N$, A and B are $(8N)\times(8N)$ matrices. Explicit formulas for A and B are given in the Appendix. Once again, the cases for $j=2$ and $j=3$ are similar.

5. Numerical examples

In this section, we consider some examples involving liquid crystals. A liquid crystal is a uniaxial medium whose relative permittivity matrix ε has two equal eigenvalues corresponding to the ordinary refractive index n_o and one different eigenvalue corresponding to the extraordinary refractive index n_e. If we assume that the optic axis (eigenvector associated with n_e) lies in the xy plane and forms an angle ϕ with the x-axis, then the elements of ε, defined in (1), are

$$\varepsilon_{11} = n_o^2 \sin^2\phi + n_e^2 \cos^2\phi, \tag{34}$$

$$\varepsilon_{12} = \varepsilon_{21} = (n_e^2 - n_o^2) \sin\phi \cos\phi, \tag{35}$$

$$\varepsilon_{22} = n_o^2 \cos^2\phi + n_e^2 \sin^2\phi. \tag{36}$$

In fact, the eigenvalues of the 3×3 matrix ε are $\varepsilon_1 = n_e^2$ and $\varepsilon_2 = \varepsilon_3 = n_o^2$. Notice that Eqs. (34)-(36) are identical to Eq. (7) with Q given in (8).

For the first example, we consider a square lattice of circular liquid crystal cylinders in vacuum. Corresponding to a phenylacetylene type liquid crystal, we let the ordinary and extraordinary refractive indices be $n_o = 1.590$ and $n_e = 2.223$ [23]. The radius of cylinders is assumed to be $a = 0.3L$, where L is the lattice constant. Using the eigenvalue problems formulated in Section 4, such as Eq. (22), we calculate the band structure on the following path of the irreducible Brillouin zone: $\Gamma X M' \Gamma X' M \Gamma$. We have performed the calculation for a few different values of ϕ including $\phi = 0$, $\pi/6$ and $\pi/4$. The results for $\phi = \pi/6$ and $N = 12$ are shown in Fig. 3. Here, N is the

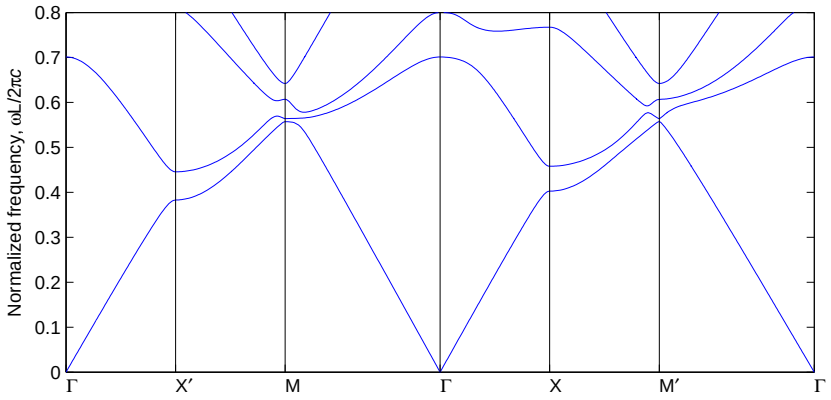

Fig. 3. Band structure of a 2D PhC composed of liquid crystal cylinders on a square lattice for $\phi = \pi/6$.

number of sampling points used on each edge of the square unit cell, therefore we only have to solve $(2N) \times (2N)$ or $(4N) \times (4N)$ matrix eigenvalue problems. To construct the DtN map, we match the special solutions inside and outside the cylinder using $J = 4N + 1$ points on the boundary. The accuracy of our results are verified by checking the convergence with respect to N. For example,

when $\omega L/(2\pi c) = 0.63$ and N is increased from 5 to 13, we observe that βL converges to 1.2697 on $\Gamma X'$ and αL converges to 2.4150 on $X'M$.

For the second example, we consider a triangular lattice of circular cylinders in a silicon background, where the cylinders are filled with a nematic liquid crystal. The radius of the cylinders is $a = 0.4L$, where L is the lattice constant. The refractive index of silicon is assumed to be $n_0 = 3.4$. The ordinary and extraordinary refractive indices of the liquid crystal are $n_o = 1.5292$ and $n_e = 1.7072$, respectively. We calculate the dispersion relations along path $\Gamma MK\Gamma M'K'\Gamma M''K''\Gamma$ as shown in Fig. 4. On each segment of the path, we solve an eigenvalue problem such as (29) or (33), involving $(4N) \times (4N)$ or $(8N) \times (8N)$ matrices. The DtN map of the unit cell is constructed using N points on each edge of the hexagon unit cell and $J = 6N + 1$ points on the boundary of the cylinder. In Fig. 4, we show our results for $N = 11$. Since the dispersion relations are calculated for real Bloch wave vectors, the eigenvalues such as η_1 in (29) and τ_1 in (33), should have a modulus exactly equal to 1. In practice, this condition is relaxed by requiring that the modulus belongs to the interval $(1 - \delta, 1 + \delta)$ for a small positive δ. For this example, a typical value for δ is $\delta = 10^{-5}$. We also check the convergence of our results with respect to N. In Table 1, we list

Table 1. Computed Bloch wave vector component for a triangular lattice of liquid crystals cylinders in a silicon background with $\omega L/(2\pi c) = 0.4$ and $\phi = \pi/4$.

N	βL for $(\alpha, \beta) \in \Gamma M'$	αL for $(\alpha, \beta) \in M'K'$
5	1.6172155	0.68074917
6	1.6185348	0.68237338
7	1.6185368	0.68251433
8	1.6185949	0.68243415
9	1.6185627	0.68239491
10	1.6185578	0.68239322
11	1.6185621	0.68239846
12	1.6185633	0.68239951
13	1.6185629	0.68239896

our results on the edges $\Gamma M'$ and $M'K'$ for various values of N. These results are obtained for the fixed normalized frequency $\omega L/(2\pi c) = 0.4$ and for a liquid crystal whose angle between the optic axis and the x axis is $\phi = \pi/4$. It is clear that 5 or 6 significant digits can be obtained using a small value of N, such as $N = 9$ or $N = 11$. For $N = 9$ and $(\alpha, \beta) \in \Gamma M'$, our linear eigenvalue problem involves only 36×36 matrices. For a comparison, we use the plane wave expansion method (MIT Photonic-Bands package) [11] to calculate the eigenfrequencies for the fixed Bloch wavevector $(\alpha L, \beta L) = (0, 1.61856)$. For the second band, the results are given in Table 2. It appears that 4 significant digits are obtained only when the number of plane waves is at least $128^2 = 16384$. In that case, the corresponding eigenvalue problem involves a 16384×16384 matrix.

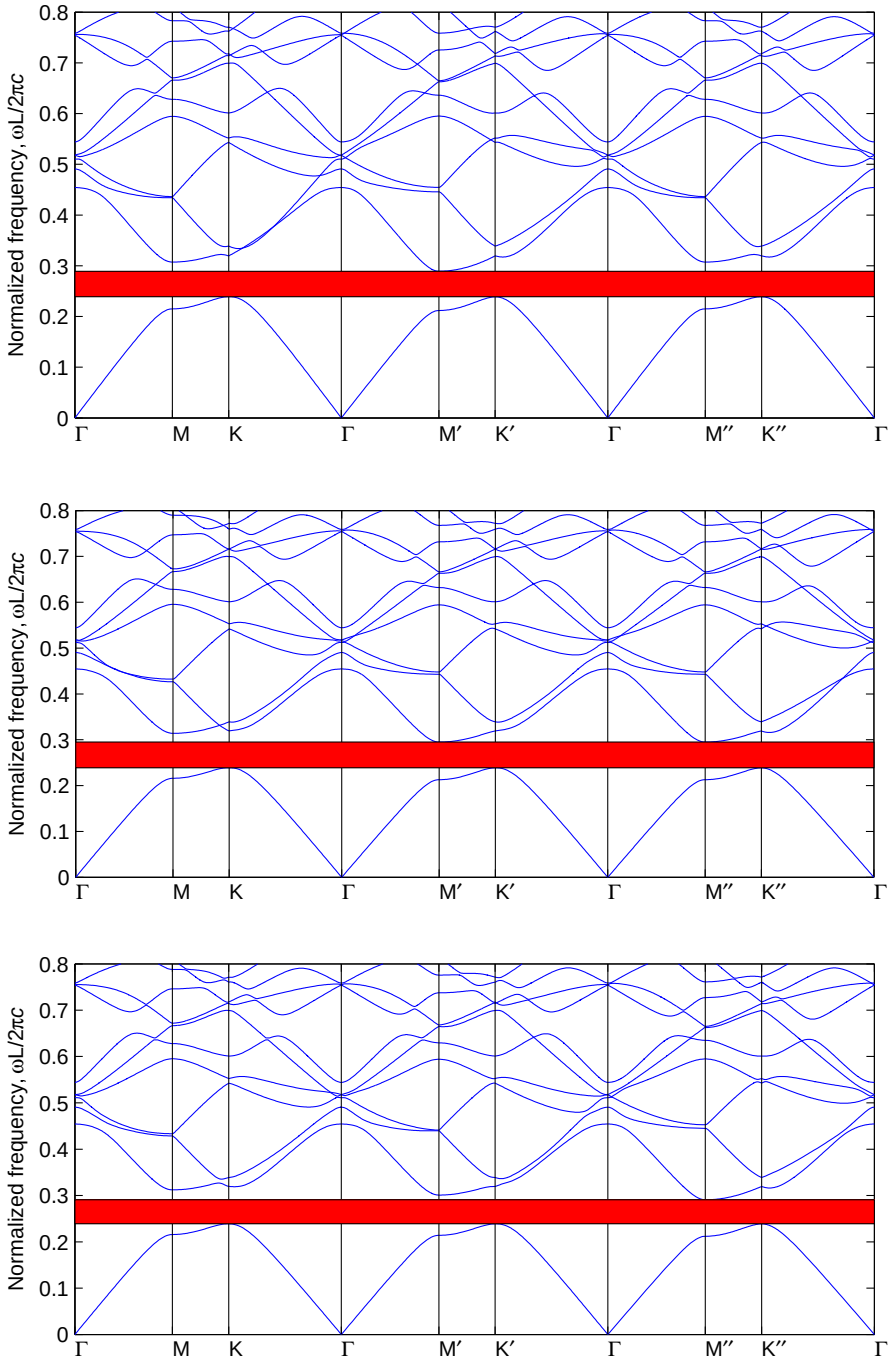

Fig. 4. Band structures of 2D photonic crystals involving a triangular lattice of circular liquid crystal cylinders in a silicon background. The angle between the optic axis of the liquid crystal and the x axis is $\phi = 0$ (top), $\phi = \pi/6$ (middle) and $\phi = \pi/4$ (bottom).

Table 2. Normalized frequency $\omega L/(2\pi c)$ of the second band for $(\alpha L, \beta L) = (0, 1.61856)$ and $\phi = \pi/4$, calculated using a plane wave expansion method.

Number of plane waves	$\omega L/(2\pi c)$ of the 2nd band
8×8	0.403271
16×16	0.399368
32×32	0.400404
64×64	0.400072
128×128	0.400034
256×256	0.400003
512×512	0.399988
1024×1024	0.399994

6. Conclusions

In this paper, we studied ideal 2D PhCs as square or triangular lattices of circular cylinders involving anisotropic media. Under the assumption that both media inside and outside the cylinders have one principle axis parallel to the axes of the cylinders, the relative permittivity matrix ε has the special form given in (1), then separation into E and H polarizations is possible. We have concentrated on the H polarization for which the governing equation (3) is different from the one for isotropic media. In Section 3, we constructed a matrix approximation for the DtN map of a unit cell involving anisotropic media, based on analytic solutions in rotated and stretched coordinates and matching the field on the boundary of the cylinder. The DtN map is then used to calculate band structures for PhCs involving liquid crystals in Sections 4 and 5. For triangular lattices, the new formulations presented in Section 4 give rise to smaller matrices compared with the original formulation described in [17]. In a typical calculation, we can obtain 5 or 6 significant digits by solving linear matrix eigenvalue problems involving $(4N) \times (4N)$ or $(8N) \times (8N)$ matrices where N is quite small, e.g. $N = 9$. The DtN map developed in Section 3 can also be used to analyze other PhC structures and devices. For example, we can follow the procedures developed in [18, 19] to analyze PhC waveguides and microcavities where the defect cells involve anisotropic media and the bulk PhC is still isotropic. We can also calculate transmission and reflection spectra for finite PhCs and solve general boundary value problems for more complicated PhC devices where some of the unit cells involve anisotropic media, using the approaches developed in [20–22].

Appendix

For a triangular lattice with a DtN map Λ given in (23) and a Bloch wave vector given as $(\alpha, \beta) = \gamma_1 \mathbf{a}_1 + \delta_1 \mathbf{b}_1$, we first write down Λ in 6×6 blocks: $\Lambda = (\Lambda_{kl})$ for $1 \le k, l \le 6$, where each block is an $N \times N$ matrix, then we solve u_0 based on the quasi-periodic condition (25) and the first and fourth rows of (23), and finally, we insert u_0 and the related u_1 into the remaining four rows of

(23). We have

$$
\begin{aligned}
D_0 &= \mu_1\Lambda_{11} - \Lambda_{41} + \mu_1^2\Lambda_{14} - \mu_1\Lambda_{44} \\
D_j &= D_0^{-1}(\Lambda_{4j} - \mu_1\Lambda_{1j}), \qquad j = 2,3,5,6, \\
M &= \begin{bmatrix} \Lambda_{22} & \Lambda_{23} & \Lambda_{25} & \Lambda_{26} \\ \Lambda_{32} & \Lambda_{33} & \Lambda_{35} & \Lambda_{36} \\ \Lambda_{52} & \Lambda_{53} & \Lambda_{55} & \Lambda_{56} \\ \Lambda_{62} & \Lambda_{63} & \Lambda_{65} & \Lambda_{56} \end{bmatrix} + \begin{bmatrix} \Lambda_{21} + \mu_1\Lambda_{24} \\ \Lambda_{31} + \mu_1\Lambda_{34} \\ \Lambda_{51} + \mu_1\Lambda_{54} \\ \Lambda_{61} + \mu_1\Lambda_{64} \end{bmatrix} [\, D_2 \quad D_3 \quad D_5 \quad D_6 \,].
\end{aligned}
$$

If δ_1 in the expression for Bloch wave vector is a constant, we insert the quasi-periodic conditions (27), (28) and (32) into Eq. (23) and obtain the linear eigenvalue problem (33), where

$$
A = \begin{bmatrix}
\Lambda_{11} & \Lambda_{12} & \Lambda_{16} & -I & 0 & 0 & 0 & 0 \\
\Lambda_{21} & \Lambda_{22} & \Lambda_{26} & 0 & -I & 0 & 0 & 0 \\
\Lambda_{31} & \Lambda_{32} & \Lambda_{36} & 0 & 0 & 0 & 0 & 0 \\
\Lambda_{41} & \Lambda_{42} & \Lambda_{46} & 0 & 0 & 0 & 0 & 0 \\
\Lambda_{51} & \Lambda_{52} & \Lambda_{56} & 0 & 0 & 0 & 0 & 0 \\
\Lambda_{61} & \Lambda_{62} & \Lambda_{66} & 0 & 0 & -I & 0 & 0 \\
0 & 0 & 0 & 0 & 0 & 0 & I & 0 \\
0 & 0 & 0 & 0 & 0 & 0 & 0 & I
\end{bmatrix},
$$

$$
B = \begin{bmatrix}
0 & -\frac{1}{\eta_1}\Lambda_{15} & -\eta_1\Lambda_{13} & 0 & 0 & 0 & -\Lambda_{14} & 0 \\
0 & -\frac{1}{\eta_1}\Lambda_{25} & -\eta_1\Lambda_{23} & 0 & 0 & 0 & -\Lambda_{24} & 0 \\
0 & -\frac{1}{\eta_1}\Lambda_{35} & -\eta_1\Lambda_{33} & 0 & 0 & \eta_1 I & -\Lambda_{34} & 0 \\
0 & -\frac{1}{\eta_1}\Lambda_{45} & -\eta_1\Lambda_{43} & 0 & 0 & 0 & -\Lambda_{44} & I \\
0 & -\frac{1}{\eta_1}\Lambda_{55} & -\eta_1\Lambda_{53} & 0 & \frac{1}{\eta_1} I & 0 & -\Lambda_{54} & 0 \\
0 & -\frac{1}{\eta_1}\Lambda_{65} & -\eta_1\Lambda_{63} & 0 & 0 & 0 & -\Lambda_{64} & 0 \\
I & 0 & 0 & 0 & 0 & 0 & 0 & 0 \\
0 & 0 & 0 & I & 0 & 0 & 0 & 0
\end{bmatrix}.
$$

Acknowledgments

This research was partially supported by a grant from the Research Grants Council of Hong Kong Special Administrative Region, China (Project No. CityU 102207).

References

1. J. D. Joannopoulos, R. D. Meade, and J. N. Winn, *Photonic Crystals: Modeling the Flow of Light* (Princeton Uiversity Press, Princeton, NJ, 1995).
2. I. H. H. Zabel and D. Stroud, "Photonic band structures of optically anisotropic periodic arrays," Phys. Rev. B **48**, 5004-5012 (1993).
3. Z. Y. Li, B. Y. Gu, and G. Z. Yang, "Large absolute band gap in 2D anisotropic photonic crystals," Phys. Rev. Lett. **81**, 2574-2577 (1998).

4. K. Busch and S. John, "Liquid-crystal photonic-band-gap materials: the tunable electromagnetic vacuum," Phys. Rev. Lett. **83**, 967-970 (1999).
5. S. W. Leonard, J. P. Mondia, H. M. van Driel, O. Toader, and S. John, "Tunable two-dimensional photonic crystals using liquid-crystal infiltration," Phys. Rev. B **61**, R2389-R2392 (2000).
6. C. S. Kee, H. Lim, Y. K. Ha, J. E. Kim, and H. Y. Park, "Two-dimensional tunable metallic photonic crystals infiltrated with liquid crystals," Phys. Rev. B **64**, 085114 (2001).
7. Y. Shimoda, M. Ozaki, and K. Yoshino, "Electric field tuning of a stop band in a reflection spectrum of synthetic opal infiltrated with nematic liquid crystal," Appl. Phys. Lett. **79**, 3627-3629 (2001).
8. C. Schuller, F. Klopf, J. P. Reithmaier, M. Kamp, and A. Forchel, "Tunable photonic crystals fabricated in III-V semiconductor slab waveguides using infiltrated liquid crystals," Appl. Phys. Lett. **82** 2767-2769 (2003).
9. M. J. Escuti, J. Qi, and G. P. Crawford, "Tunable face-centered-cubic photonic crystal formed in holographic polymer dispersed liquid crystals," Opt. Lett. **28**, 522-524 (2003).
10. S. F. Mingaleev, M. Schillinger, D. Hermann, and K. Busch, "Tunable photonic crystal circuits: concepts and designs based on single-pore infiltration," Opt. Lett. **29**, 2858-2860 (2004).
11. S. G. Johnson and J. D. Joannopoulos, "Block-iterative frequency-domain methods for Maxwell's equations in a planewave basis," Opt. Express **8**, 173-190 (2001).
12. M. Marrone, V. F. Rodriguez-Esquerre and H. E. Hernández-Figueroa, "Novel numerical method for the analysis of 2D photonic crystals: the cell method," Opt. Express **10**, 1299-1304 (2002).
13. P. J. Chiang and C. P. Yu and H. C. Chang, "Analysis of two-dimensional photonic crystals using a multidomain pseudospectral method," Phys. Rev. E **75**, 026703 (2007).
14. S. M. Hsu, M. M. Chen, and H. C. Chang, "Inverstigation of band structures for 2D non-diagonal anisotropic photonic crystals using a finite element method based eigenvalue algorithm", Opt. Express **15**, 5416-15430 (2007).
15. A. Taflove and S. C. Hagness, *Computational Electrodynamics: The Finite-Difference Time-Domain Method* (2nd ed., Artech House, 2000).
16. J. Yuan and Y. Y. Lu, "Photonic bandgap calculations using Dirichlet-to-Neumann maps," J. Opt. Soc. Am. A **23**, 3217-3222 (2006).
17. J. Yuan and Y. Y. Lu, "Computing photonic band structures by Dirichlet-to-Neumann maps: The triangular lattice," Opt. Commun. **273**, 114-120 (2007).
18. Y. Huang, Y. Y. Lu and S. Li, "Analyzing photonic crystal waveguides by Dirichlet-to-Neumann maps," J. Opt. Soc. Am. B **24**, 2860-2867 (2007).
19. S. Li and Y. Y. Lu, "Computing photonic crystal defect modes by Dirichlet-to-Neumann maps," Opt. Express **15**, 14454-14466 (2007).
20. Y. Huang and Y. Y. Lu, "Scattering from periodic arrays of cylinders by Dirichlet-to-Neumann maps," J. Lightwave Technol. **24**, 3448-3453 (2006).

21. Y. Wu and Y. Y. Lu, "Dirichlet-to-Neumann map method for analyzing interpenetrating cylinder arrays in a triangular lattice," J. Opt. Soc. Am. B **25**, 1466-1473 (2008).
22. Z. Hu and Y. Y. Lu, "Efficient analysis of photonic crystal devices by Dirichlet-to-Neumann maps," Opt. Express **16**, 17383-17399 (2008).
23. H. Takeda and K. Yoshino, "TE-TM mode coupling in two-dimensional photonic crystals composed of liquid-crystal rods," Phys. Rev. E **70**, 026601 (2004).
24. S. M. Hsu and H. C. Chang, "Full-vectorial finite element method based eigenvalue algorithm for the analysis of 2D photonic crystals with arbitrary 3D anisotropy," Opt. Express **15**, 15797-15822 (2007).
25. G. Alagappan, X. W. Sun, and P. Shum, "Symmetry properties of two-dimensional anisotropic photonic crystals," J. Opt. Soc. Am. A **23**, 2002-2013 (2006).
26. J. Yuan, Y. Y. Lu, and X. Antoine, "Modeling photonic crystals by boundary integral equation and Dirichlet-to-Neumann maps," J. Comput. Phys. **9**, 4617-3629 (2008).